

CeBr₃ gamma-ray logging probe qualification for uranium mining applications

Thomas Marchais^{1,*}, Bertrand Pérot¹, Hervé Toubon², Youcef Bensedik², Romain Mieszkalski², Sebastien Hocquet², Dragomir Savov², Matthew Schubert³, Bruno Legros³, Patrick Van Eyll³, Michaël Pernette³

¹CEA, DES, IRESNE Institute, DTN, SMTA, Nuclear Measurement Laboratory, France

²Orano Mining, France

³Advanced Logic Technology, Luxembourg

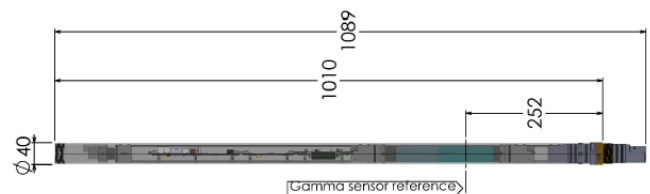
* Corresponding author: Thomas.MARCHAIS@cea.fr

Abstract— The development and optimization of gamma-ray spectrometry tools are crucial for ORANO Mining and geophysical exploration. This study presents a comprehensive study on the ALT QL40-SGR-2G spectrometric probe, equipped with a cerium bromide (CeBr₃) detector, aimed at its detailed characterization and the validation of its numerical model through various experimental setups and MCNP (Monte Carlo N-Particle) simulations. The study described energy calibration, resolution and detection efficiency measurements at a 15 cm distance, crystal length characterization, probe rotation effects on performance, counting loss estimation, and response profile determination in a sand silo setup. These experiments aimed to validate the MCNP model of the probe and understand factors affecting its performance. Utilizing standard gamma sources, energy resolution and detection efficiency of the probe were evaluated, revealing a close match between experimental data and MCNP calculations, with a 2.4% average discrepancy across the energy spectrum. This validation highlights the reliability of the numerical model and the robustness of the probe in diverse measurement scenarios. Further investigations on the effective length of crystal confirmed the manufacturer's specifications, while tests on the probe's rotational impact showed minimal effect on spectral response (< 4%). The use of the 2 sources method allowed for accurate dead time estimation, which is crucial for correcting counting losses in high-radiation environments. In addition, this study involved the spatial response of the probe using a ¹³⁷Cs source within a sand silo. This experiment demonstrated the potential of this probe in simulating complex geological formations and validated the MCNP model accuracy in predicting spatial response, which is crucial for borehole modelling. The successful correlation between experimental findings and MCNP simulations enhances confidence in using the QL40-SGR-2G probe for accurate gamma-ray detection and analysis in varied settings.

Index Terms— CeBr₃(Ce) probe for uranium borehole logging, MCNP simulation, experimental calibration, dead time

I. INTRODUCTION

The ALT QL40-SGR-2G probe, which is used for detecting gamma emissions within a wellbore, employs either a CeBr₃ or BGO. For this study, we utilized a CeBr₃ detector measuring 20 mm x 96 mm. Fig. 1 illustrates the probe's design, which is 1089 mm long.



QL40-SGR-2G

Fig. 1. QL40-SGR-2G CeBr₃ probe.

This spectrometric probe was partially qualified in a previous study [1] on a standard block in Bessines, France [2], [3]. A significant discrepancy was observed in the total counting rate at high uranium content between MCNP [4] numerical simulations and experimental results. Consequently, it was decided to further characterize the probe in the Nuclear Measurement Laboratory at CEA Cadarache using standard sources. This process involved several steps:

- energy calibration, estimation of the probe's resolution and its detection efficiency at a distance of 15 cm, that permitted to compare experimental data with calculations performed using MCNP transport code,
- measurement of the crystal's length using a motorized table,
- assessment of the effect of the probe rotation on its performance,
- estimation of counting losses using the two-source method,
- determination of the response profile in a sand silo.

The results of the previous highlighted points are presented in the subsequent sections, allowing for the qualification of the MCNP model of the probe and the estimation of various influential factors intrinsic to the probe.

II. LABORATORY QUALIFICATION

A. Energy resolution and detection efficiency

To characterise the energy calibration of the probe, its resolution and its detection efficiency at 15 cm, we used six standard sources available in the laboratory: ⁶⁰Co, ⁸⁸Y, ¹³³Ba, ¹³⁷Cs, ¹⁵²Eu, and ²⁴¹Am. Table 1 shows the characteristics

emission of each standard sources. It should be noted that the gamma emissions have been selected to have no parasitic lines.

TABLE I
MAIN GAMMA EMISSION OF SIX STANDARDS SOURCES [5]

Source	Activity (Bq)	Gamma energy (keV)	Gamma intensity (%)
⁶⁰ Co	28.2 x 10 ³	1173.23	99.85
		1332.49	99.98
⁸⁸ Y	10.1 x 10 ³	898.04	93.7
		1836.07	99.35
¹³³ Ba	29.9 x 10 ²	356.01	62.05
¹³⁷ Cs	33.5 x 10 ³	661.66	85.01
¹⁵² Eu	40.1 x 10 ³	121.78	28.41
		244.70	7.55
		344.28	26.59
		964.08	14.50
²⁴¹ Am	60.2 x 10 ³	59.54	35.92

Fig. 2 shows the experimental configuration and corresponding measured spectra, with 2048 channels, for the six standards sources. These six sources are positioned 15 cm from the centre of the crystal.

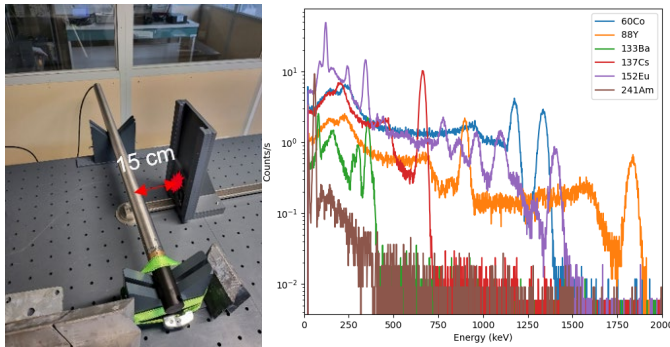


Fig. 2. Geometry of 6 sources measurement and corresponding spectra.

The previous spectra were calibrated thanks to the well-known emission lines of the 6 standard sources, see Table I. Thanks to this calibration, a 2-h background measurement without radioactive sources was carried out, see Fig. 3. This measurement shows that no contribution of background noise is to be noted in the selected lines of this study. In addition, we can clearly see the characteristic peaks of a background noise, 1460 keV from ⁴⁰K and 609 keV from ²¹⁴Bi.

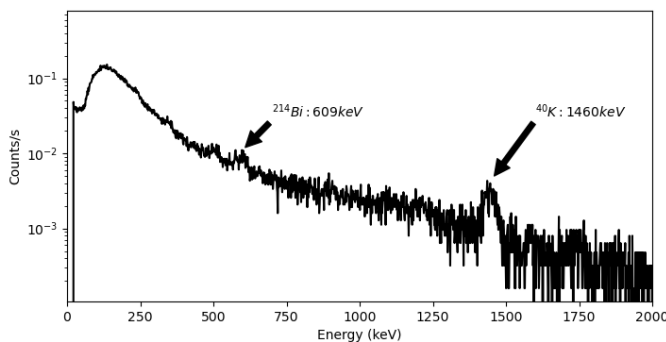


Fig. 3. Background noise spectrum

The energy resolution, denoted as FWHM (Full Width at Half Maximum), is estimated for each Gaussian peak and can be expressed by the following formula:

$$FWHM(E) = A + B \times \sqrt{E + C \times E^2} \quad (1)$$

With:

- E: the energy of the Gaussian peak in keV,
- A, B, C: three coefficients respectively in keV, keV^{1/2} and keV⁻¹.

The following figure shows the FWHM estimated thanks to the 6 sources measurements and formula (1). In addition, an example of Gaussian curve fitting is provided for the characteristic gamma emission at 662 keV from ¹³⁷Cs.

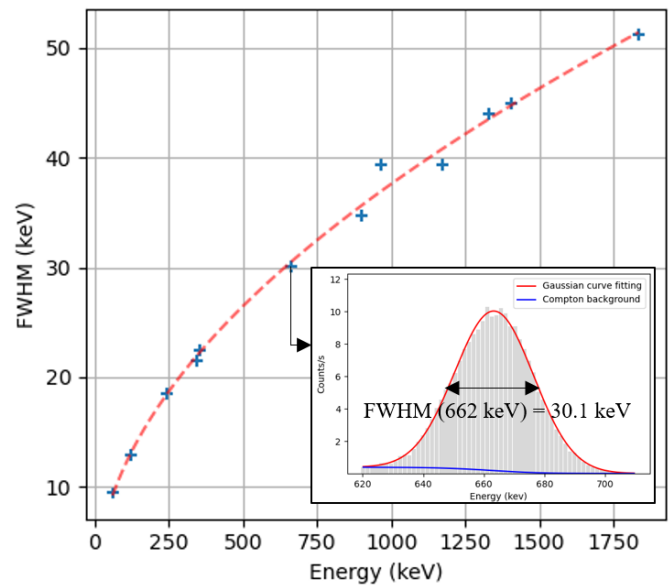


Fig. 4. Energy resolution of the probe as function of the energy and example of gaussian curve fitting for the characteristic gamma emission at 662 keV from ¹³⁷Cs.

We notice an energy resolution of 4.5% (30.1 keV) at 662 keV from ¹³⁷Cs source. This resolution corresponds to the classic resolution of a CeBr3 detector [6]. For equation (1), we found A = 0.22 keV, B = 1.17 keV^{1/2} and C = 2.70 x 10⁻⁵ keV⁻¹.

The detection efficiency, denoted *Eff*(15 cm), is estimated for each peak according:

$$Eff(15\text{ cm}) = \frac{Sn(E)}{Act(S) \cdot I(E)} \quad (2)$$

With:

- *Sn*(E): net area of the Gaussian peak
- *Act*(S): activity of the source, see Table 1,
- *I*(E): gamma intensity at energy E, see Table 1.

In addition, and in order to compare with simulated values, we decided to simulate the geometry of measurement with MCNP6 transport code [4], see Fig. 5. The objective is to validate the numerical model of the CeBr₃ probe. This modelled geometry is based on manufacturer characteristics and has already been used to model concrete blocks of increasing uranium

content [1]. We subsequently modelled the measurement geometry of the 6 point sources described in part A.

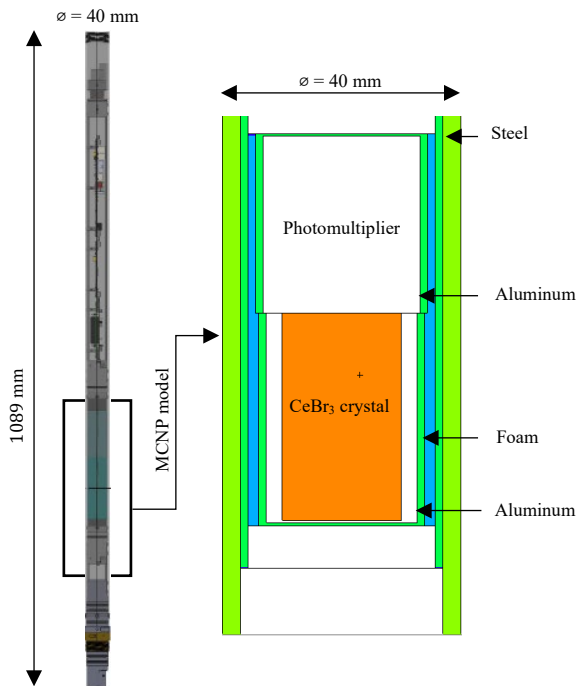


Fig. 5. QL40-SGR-2G probe from Advanced Logic Technology (ALT) and its associated MCNP model.

The following figure shows the detection efficiency of the probe at 15 cm, estimated through the measurements from six sources and formula (2), with the experimentation shown in red and MCNP calculations depicted in blue. The uncertainty plotted for the experimental values includes those due to statistical uncertainty and the activity of standard sources (3%). The uncertainty on the MCNP values is not visible on the figure because of very low values (<1%).

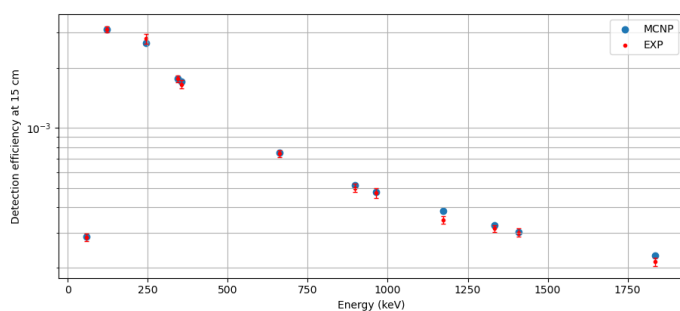


Fig. 6. Detection efficiency of the probe at 15 cm for experimental values and MCNP calculations.

The previous figure shows a very good agreement between the experiment and the MCNP calculation with only a 2.4% average discrepancy across the entire energy range.

B. Detector length estimation

To ascertain the length of the crystal but also its uniformity of response, we utilised a 1 mm collimated slit of lead, a ^{137}Cs

source, and a motorised table which, through 42 measurements, enabled us to estimate the crystal's length with a step of 1 mm. The uncertainty in the measured crystal dimension is 2 mm, attributable to the distance between the probe and the source, as well as the collimated slit.

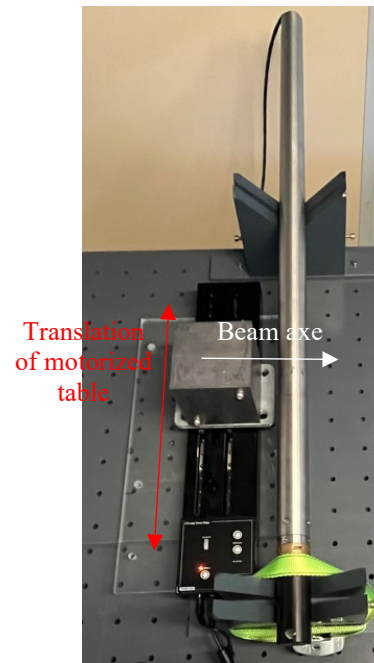


Fig. 7. Motorized table for fine characterization of the CeBr3 probe crystal.

The following figure illustrates, for the 42 measurements, the net area of the 662 keV peak of ^{137}Cs as a function of the position of the source.

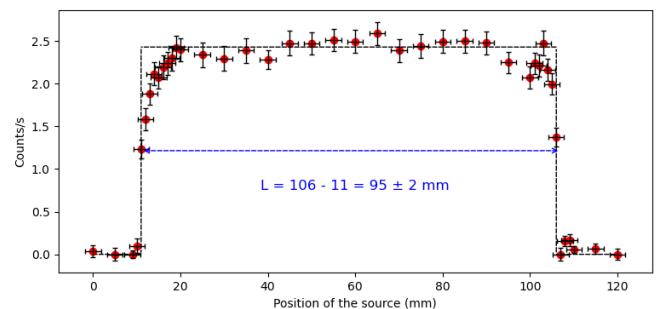


Fig. 8. Net area of the 662 keV peak from ^{137}Cs source for 42 measurement points.

A crystal length of 95 ± 2 mm was determined, which is in good agreement with the manufacturer's data (96 mm). The uniformity of the probe's response over the length of its crystal is relatively good. The fluctuations in the net area observed when we are in the crystal, between 11 mm and 106 mm, are attributable to the presence of absorbing elements close to the crystal or to a poor collection of charges inside it.

C. Probe rotation effect

In order to examine the uniformity of the spectral response of the CeBr₃ probe whilst it was rotated within the borehole, we opted to rotate the probe about its axis at a pitch of 45°.

Throughout these measurements, sources of ^{137}Cs , ^{60}Co , and ^{88}Y were employed at the same time to characterise the angular response across an energy spectrum ranging from 662 keV (^{137}Cs) to 1836 keV (^{88}Y). The subsequent figure illustrates the deviation for each net area estimated relative to the mean value. Moreover, the total count rate is also presented in the case of using the probe in total count rate mode. The uncertainty plotted for the experimental values includes those due to statistical uncertainty ($\approx 1\%$).

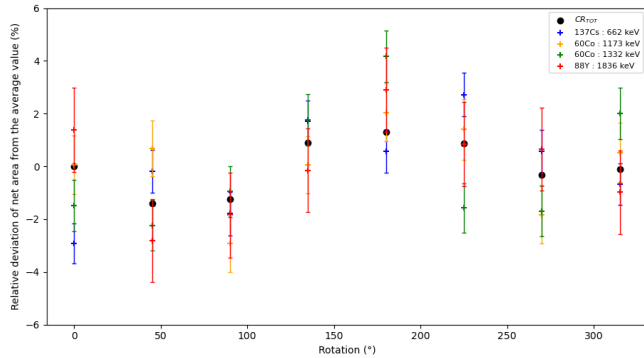


Fig. 9. Probe rotation effect of the signal of 3 standards sources (^{137}Cs , ^{60}Co , and ^{88}Y) and total count rate.

We can observe a very low effect of rotation ($< 4\%$) for each point of measurement. The effect of rotation is lower than 1% for the total count rate.

D. Counting loss and dead time

In order to verify the dead time correction carried out by the CeBr_3 probe, it was decided to quantify the counting losses using the “2 sources” method [7]:

- a reference source of ^{137}Cs is placed at a fixed position near the CeBr_3 probe, which emits gamma radiation at 662 keV not coinciding with any other emission from the second source used (^{60}Co). The net area at 662 keV on the reference spectrum is $S_{\text{Ref}} = 210 \text{ counts}\cdot\text{s}^{-1}$, for a total counting rate of 1073 $\text{counts}\cdot\text{s}^{-1}$ and a dead time of 0.16% when no disturbing source is not used.
- a disturbing source of ^{60}Co is then approached as the detector progresses in order to increase the total counting rate and the dead time. Six positions of the disturbing source, so six total count rates, have been measured. At each step, we measure the net area at 662 keV due to the reference source. Upon contact with the probe, the disturbing source induces a counting rate of 167,200 $\text{counts}\cdot\text{s}^{-1}$ and a dead time of 16.35%.

The following figure represents the counting losses in the net area at 662 keV as a function of the total counting rate on the spectra. Each measurement is carried out for an active time of 120 seconds.

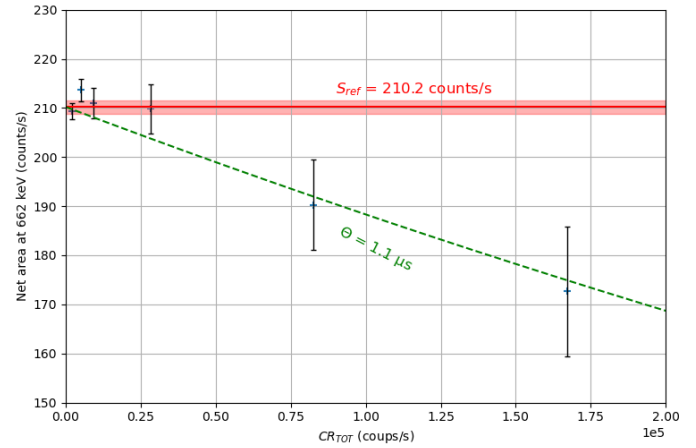


Fig. 10. Counting losses in the net area at 662 keV as a function of the total counting rate. In red the value of the net area at 662 keV when the ^{137}Cs source is alone. In green, the adjustment made to the data to estimate the dead time.

Thanks to these measurements, we are able to accurately estimate the dead time θ , of this probe (green curve in Fig. 10). The paralyzable model [7] can be directly used to estimate the dead time.

$$Sn(662 \text{ keV}) = S_{\text{ref}} \times e^{-CR_{\text{TOT}} \times \theta} \quad (3)$$

With:

- $Sn(662 \text{ keV})$: net area at 662 keV, in $\text{counts}\cdot\text{s}^{-1}$,
- S_{ref} : net area at 662 keV on the reference spectrum without disturbing source, $S_{\text{ref}} = 210 \text{ counts}\cdot\text{s}^{-1}$,
- CR_{TOT} : total count rate, in $\text{counts}\cdot\text{s}^{-1}$,
- θ : dead time, in second.

We found a $\theta = 1.1 \mu\text{s}$ with this experimentation (see green curve in Fig. 10). This value is in relative good agreement with the manufacturer's data, $\theta = 0.8 \mu\text{s}$.

E. Spatial response of the probe in a sand silo

Finally, to complete the characterization of the CeBr_3 probe, we decided to study its spatial response to a mono-energetic source of ^{137}Cs in a sand silo. This source was selected because of this gamma emission at 662 keV, near to the characteristic peak of a uranium decay chain at 609 keV of ^{214}Bi . For this, we used a Fontainebleau sand silo, already used in previous studies for measurements using a neutron probe [8]. This silo, shown in Fig. 11, with a weight of 1.5 tonnes, measures 1.50 metres high and has an internal diameter of 100 cm. The density of the matrix is equal to 1.6. Four smaller stainless steel tubes, each 6 cm in diameter, are positioned at different radial distances ($n^\circ 1$: 13.2 cm, $n^\circ 2$: 22.7 cm, $n^\circ 3$: 32.7 cm, and $n^\circ 4$: 47 cm) from the centre to introduce the ^{137}Cs source.

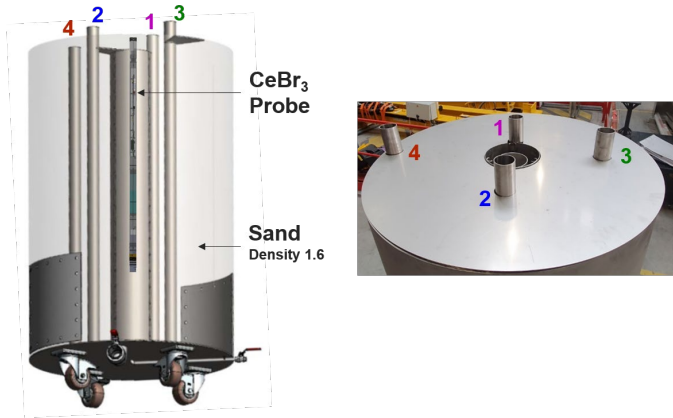


Fig. 11. On the left, the silo as well as the position of the probe and the 4 instrumentation tubes. On the right, a photograph of the top of the silo in order to observe the position of the 4 tubes used to insert the Cs source

At the same time, an MCNP model of the sand silo was developed using the CeBr₃ probe model presented previously in order to validate the simulated response of the probe in a real environment, see Fig. 12.

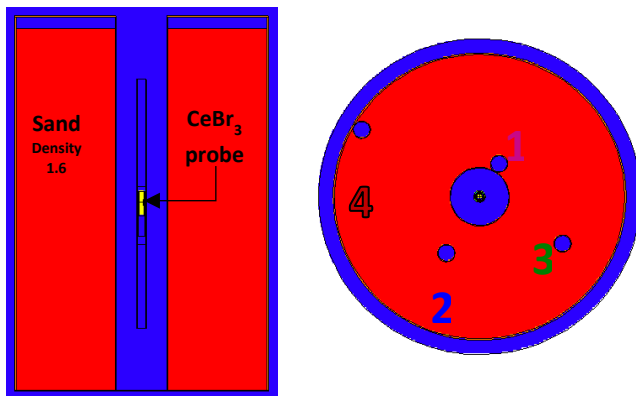


Fig. 12 : MCNP model of the sand silo

The Fig. 13, compares, for the 4 positions of the instrumentation tube (n°1, n°2, n°3, and n°4) and various depths of the source within the silo, the MCNP predictions and the measurements. All values were normalized to the value of 110 cm, corresponding to the position where the centre of the crystal is directly in front of the source, to facilitate comparison of each profile within the same figure.

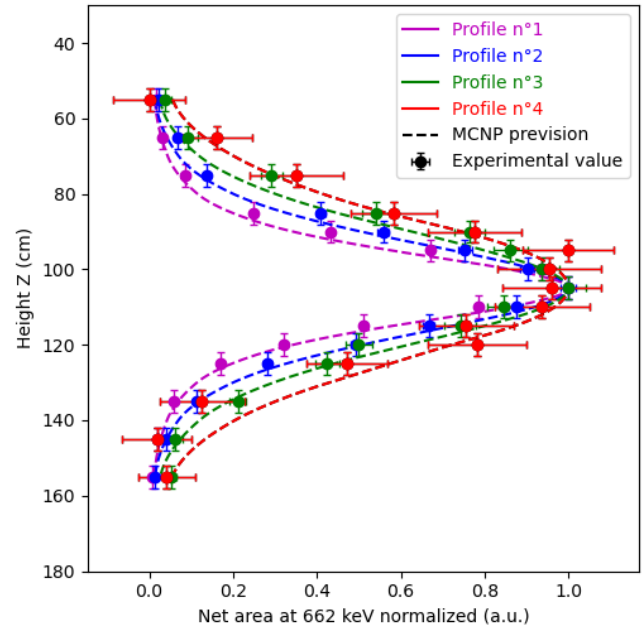


Fig. 13. Axial response of the CeBr₃ probe

The axial response of the probe is modelled with high accuracy by MCNP. The Table 2 displays the full width at half maximum (FWHM) of each profile, detailing both the experimental values, denoted as FWHM_{EXP}, and the MCNP estimations, referred to FWHM_{MCNP}.

TABLE II
Comparison of axial response (FWHM) between MCNP calculation and experimental value

Profile	FWHM _{EXP} (cm)	FWHM _{MCNP} (cm)	$\frac{FWHM_{MCNP} - FWHM_{EXP}}{FWHM_{EXP}}$
n°1	25.8	25.8	0.0%
n°2	33.5	32.6	-2.7%
n°3	41.4	38.8	-6.3%
n°4	43.0	46.0	7.0%

We notice that the full width at half maximum of each profile response increases following the distance from the probe. For example, the FWHM_{EXP} = 25.8 cm for the profile closest to the probe while FWHM_{EXP} = 46 cm for the profile farthest from the centre of the silo.

III. CONCLUSIONS

A comprehensive series of laboratory tests and simulations were used in this study to characterization the ALT QL40-SGR-2G spectrometric probe, equipped with a CeBr₃ detector. The investigation explored crucial points such as energy resolution, detection efficiency, crystal length, probe rotation effects, counting losses, and spatial response in a sand silo context. The experimental results obtained demonstrated the probe's capabilities and reliability in various conditions, but also validated its MCNP numerical model.

The numerical model and probe design are robust due to their close agreement with experimental data and MCNP simulations, particularly in detection efficiency (2.4%) and spatial response characterization. Thanks to this study, we can now use the probe in a wider range of geophysical application and environmental monitoring tasks, with enhanced confidence in the accuracy of its measurements and the interpretations derived from them. The validated MCNP model can be further utilized to explore more complex geological scenarios, including heterogeneous formations and those with varying levels of radioactivity. The use of advanced modelling can lead to the creation of more sophisticated algorithms for the identification and quantification of materials in the subsurface.

REFERENCES

- [1] T. Marchais *et al.*, “Experimental validation of a CeBr₃ gamma-ray logging probe MCNP model,” *EPJ Web Conf.*, vol. 288, p. 05003, 2023, doi: 10.1051/epjconf/202328805003.
- [2] “Detailed MCNP Simulations of Gamma-Ray Spectroscopy Measurements With Calibration Blocks for Uranium Mining Applications | IEEE Journals & Magazine | IEEE Xplore.” Accessed: Feb. 08, 2024. [Online]. Available: <https://ieeexplore.ieee.org/document/8268552>
- [3] B. Pérot *et al.*, “Development of Gamma Spectroscopic Tools for Uranium Ore Samples and Borehole Exploration,” in *2022 IEEE Nuclear Science Symposium and Medical Imaging Conference (NSS/MIC)*, Italy: IEEE, Nov. 2022, pp. 1–5. doi: 10.1109/NSS/MIC44845.2022.10398898.
- [4] Los Alamos National Laboratory, “MCNP6, User’s manual – Version 1.0 - LA-CP-13-00634, Rev. 0 – May 2013 – Denise B. Pelowitz, editor.” 2013.
- [5] M. M. Be, Ch. Dulieu, and V. Chiste, “NUCLEIDE-LARA, a library for alpha, X and gamma emissions sorted by increasing energy,” France, 2008.
- [6] F. G. A. Quarati *et al.*, “Scintillation and detection characteristics of high-sensitivity CeBr₃ gamma-ray spectrometers,” *Nucl. Instrum. Methods Phys. Res. Sect. Accel. Spectrometers Detect. Assoc. Equip.*, vol. 729, pp. 596–604, Nov. 2013, doi: 10.1016/j.nima.2013.08.005.
- [7] G. F. Knoll, *Radiation detection and measurement*, 3rd ed. New York: Wiley, 2000.
- [8] V. Fondement *et al.*, “Development of a neutron probe to perform a combined measurement of uranium concentration and hydrogen porosity for mining applications,” *Nucl. Instrum. Methods Phys. Res. Sect. Accel. Spectrometers Detect. Assoc. Equip.*, vol. 1059, p. 168888, Feb. 2024, doi: 10.1016/j.nima.2023.168888.